Supplementary Information for

Anti-poisoning defective catalyst without metal active sites for NH_3-SCR via in-situ stabilization

Ge Li[1,†], Baodong Wang[1,2,,†], Ziran Ma[1,*], Jing Ma[1], Hongyan Wang[1], Jiali Zhou[1], Shengpan Peng[1], Jessica Jein White[3], Yonglong Li[1], Jingyun Chen[1], Zhihua Han[1], Hui Wei[1], Chuang Peng[4], Yujie Xiong[5,*], Yun Wang[3,*]*

1National Institute of Clean-and-Low-Carbon Energy; Beijing 102211, China

2 NICE Europe Research GmbH, Stockholmer Platz 1, Stuttgart 70173 , Germany

3Centre for Catalysis and Clean Energy, School of Environment and Science, Gold Coast Campus, Griffith University; Queensland 4222, Australia

4School of Resource and Environmental Sciences and Hubei International Scientific and Technological Cooperation Base of Sustainable Resource and Energy, Wuhan University; Wuhan 430072, China

5School of Chemistry and Materials Science, University of Science and Technology of China; Hefei, Anhui 230026, China

This PDF file includes:

Figs. S1 to S25

Tables S1 to S5

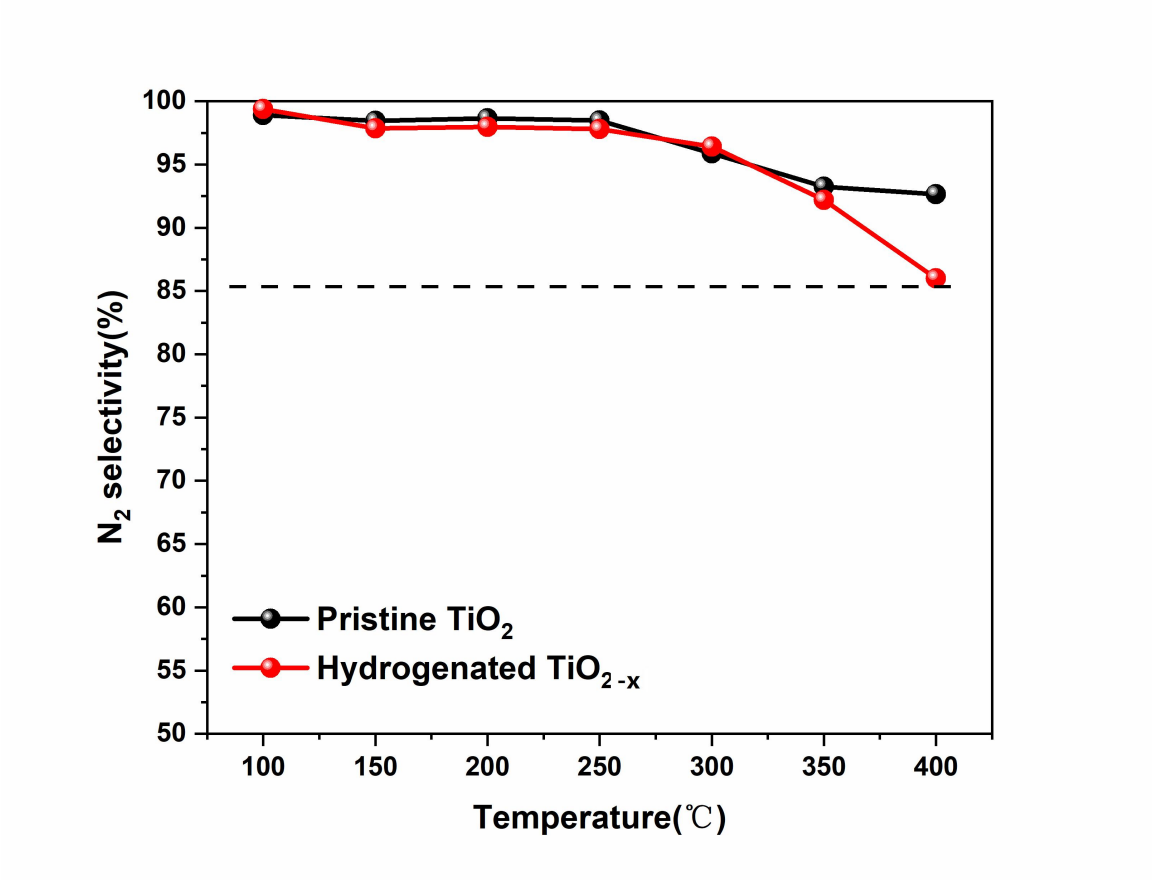

Fig.S1. N_2 selectivity of hydrogenated TiO_{2-x} catalysts

The selectively for N_2 was essentially unchanged after hydrogenation, remaining above 87.5%.

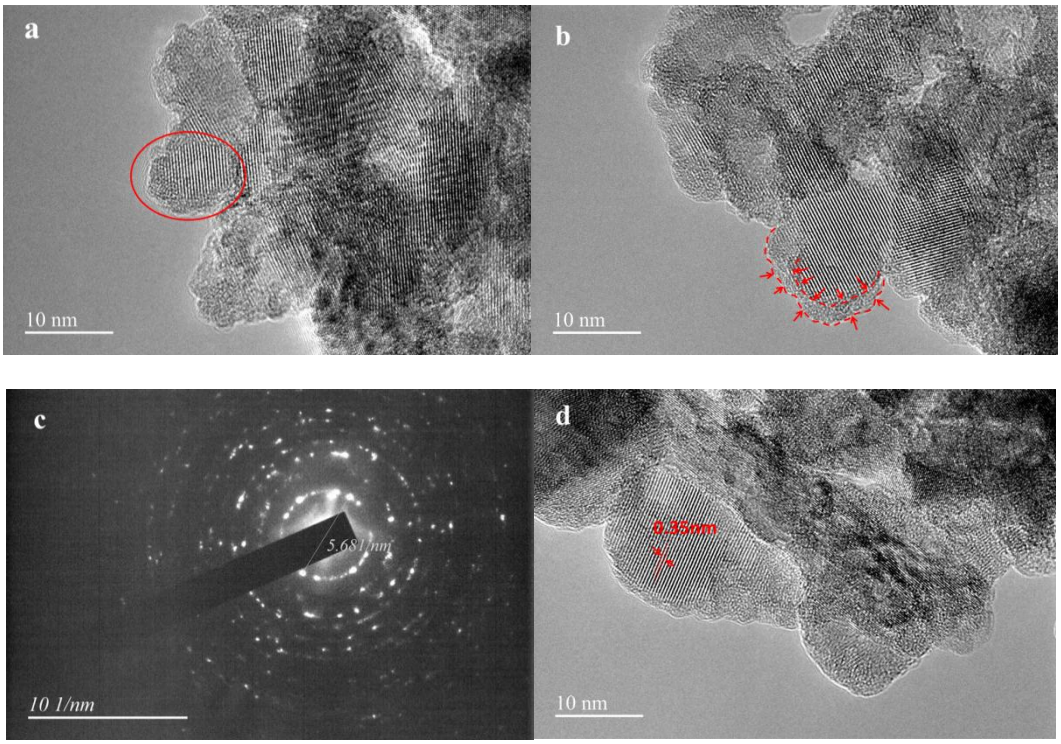

Fig.S2. HRTEM images of hydrogenated TiO_{2-x} nano-powders.

The H-TiO_{2-x} nanoparticles were found to have an anatase crystalline/disordered core–shell structure with a 1.75-2.63 nm thick disordered surface layer. The interplanar lattice spacing of hydrogenated TiO_2 was about 0.35 nm, which corresponded to that of the (101) plane of anatase (0.325 nm).

Chemical composition analysis results of the synthesized pristine titanium dioxide and hydrogenated TiO_{2-x} are listed in Table S1.

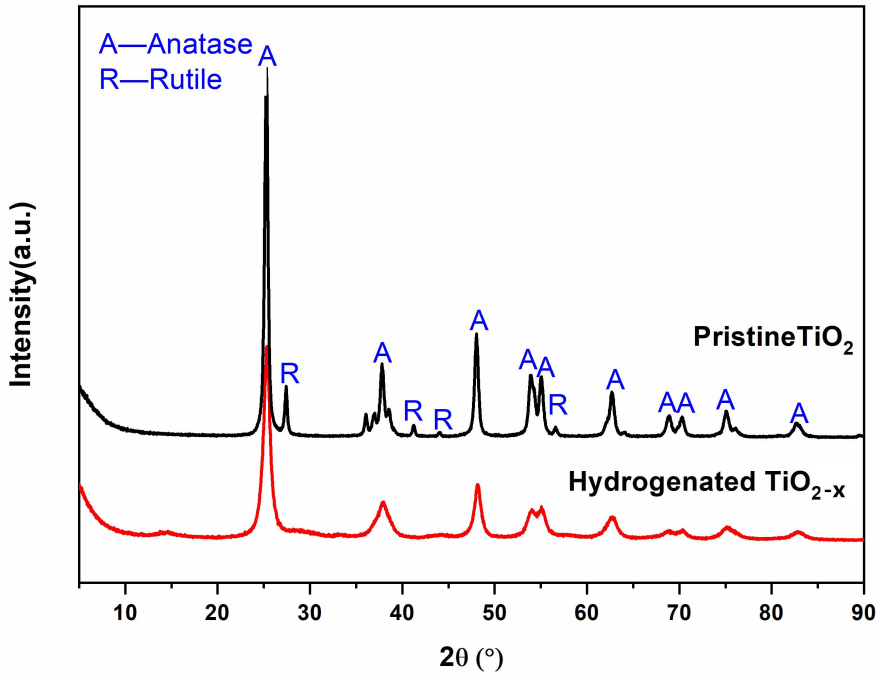

Fig. S3. XRD patterns of hydrogenated TiO_{2-x} catalyst and pristine TiO_2.

The phase composition of the pristine TiO_2 was primarily anatase and 6.84% rutile. However, after hydrogenation, the rutile diffraction peaks disappeared with only the anatase phase remaining. Rutile is much easier to reduce to hydrogenated TiO_{2-x} compared with anatase. As the Ti–O distances (0.1949 and 0.1980 nm) in rutile are greater than those in anatase (0.1934 and 0.1980 nm), O is easier to separate from the TiO_2 crystal in rutile. The anatase diffraction peaks were also clearly broadened and less intense, indicating that the size and structure of the crystal had changed significantly. The average crystal size of the H-TiO_{2-x} was estimated to be 17.34 nm using the Scherrer equation.This was due to trivalent Ti and O vacancies being produced during the hydrogenation reduction process.

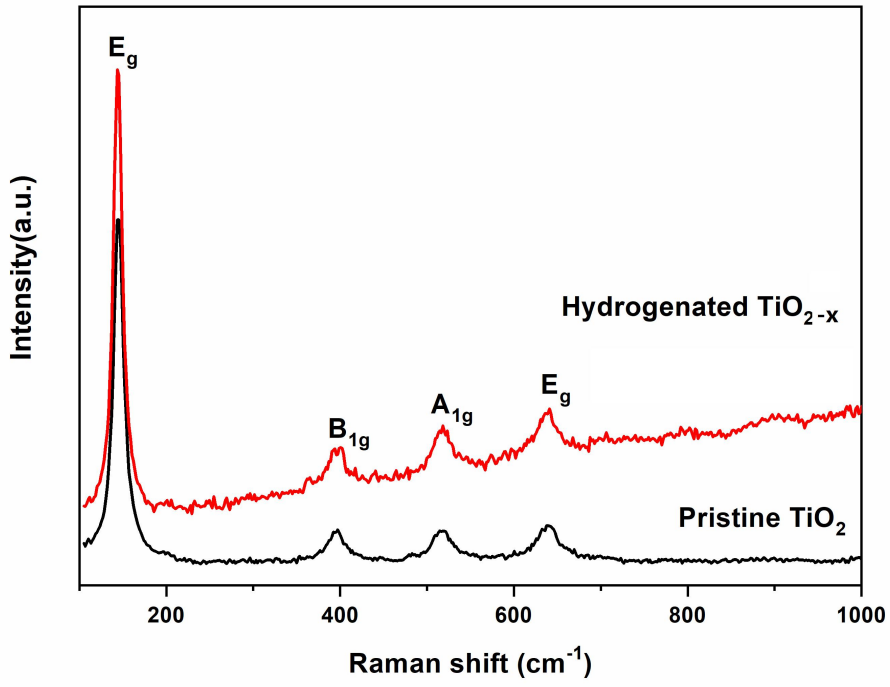

Fig. S4. Raman spectra of hydrogenated TiO_{2-x} catalyst and pristine TiO_2.

Raman spectra of pristine TiO_2 and hydrogenated TiO_{2-x} nanoparticles are shown in Fig. S4. Raman active modes located at ~143cm^{-1} (E_g), 395cm^{-1} (B_{1g}), 520cm^{-1} (A_{1g}), and 641 cm^{-1} (E_g) were detected for all samples, indicating that all samples were mainly composed of anatase phase. However, the scattering peaks of hydrogenated TiO_2 were broadened and shifted toward higher wavenumbers. The presence of defects was somewhat responsible for the blue-shift and broadening of the peaks.

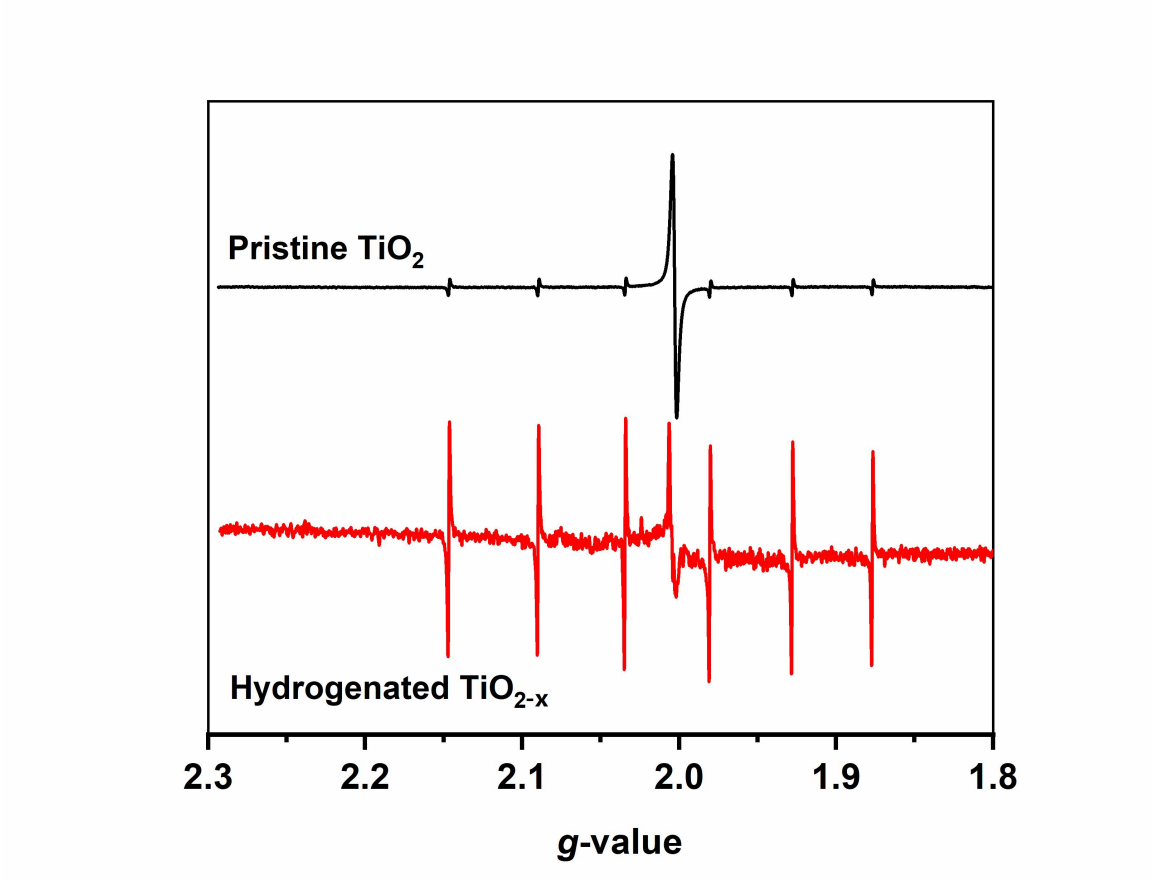

Fig. S5. EPR spectra of hydrogenated TiO_{2-x} catalyst and pristine TiO_2.

Figure S5 shows the EPR spectra of hydrogenated TiO_{2-x} catalyst and pristine TiO_2 measured at 293 K and ambient pressure. The reported g values for Ti^{3+} on the surface or in the bulk of TiO_2 are 2.02–2.03 and 1.978, 1.959, respectively. In the hydrogenated TiO_{2-x}, the peak at g<2 was attributed to oxygen vacancy (V_O*) Ti^{3+}. According to the chemical equilibrium, one Ti^{3+} and two Ti^{2+} are generated by the generation of oxygen vacancies. As shown in Fig. S5, more (V_O*) Ti^{3+} peaks were present after hydrogenation, indicating that additional oxygen vacancies were generated on the surface of the material, which is more conducive to oxygen conduction in the denitrification reaction.

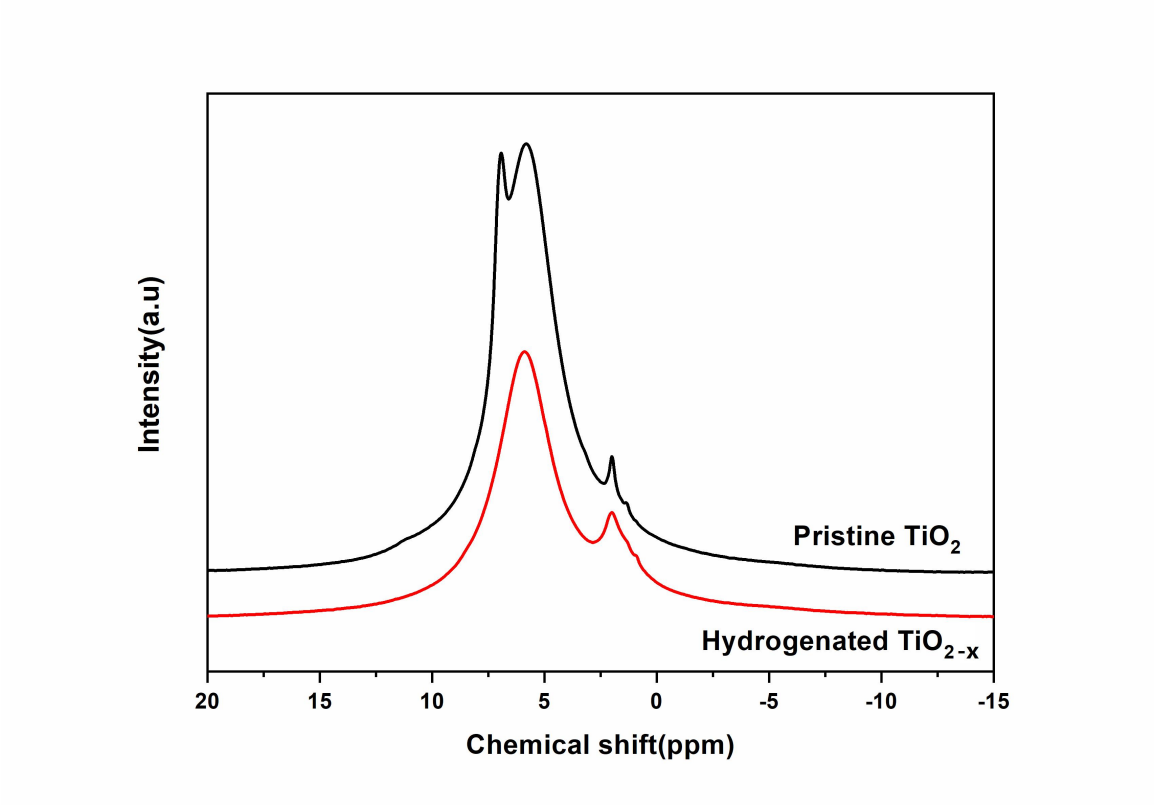

Fig. S6. ^{1}H NMR spectra of hydrogenated TiO_{2-x} catalyst and pristine TiO_2.

Figure S6 shows the ^{1}H NMR spectra of pristine TiO_2 and hydrogenated TiO_{2-x}. The chemical shift at 5–7 ppm was attributed to surface-adsorbed water, while that at 2 ppm was attributed to $H–O_{3C}$ functional groups on the TiO_2 surface. The content of surface-adsorbed water was significantly reduced, while that of $H–O_{3C}$ functional groups on the surface was significantly increased, after hydrogenation, which was due to the presence of hydrogen in the disordered surface layer resulting from hydrogenation.

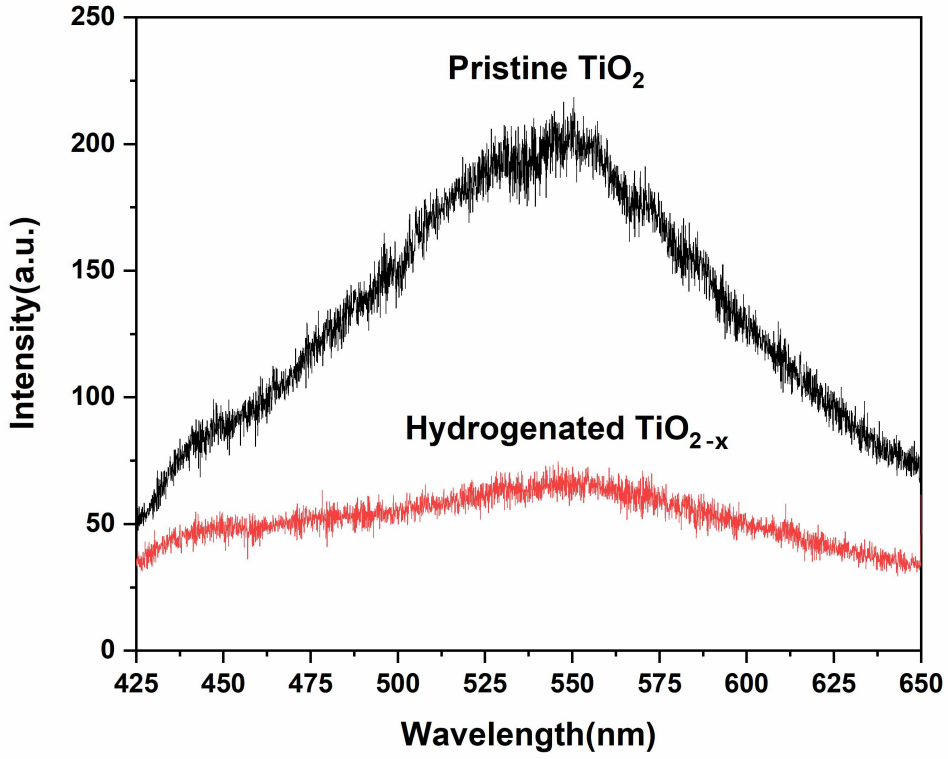

Fig. S7. Photoluminescence spectra of hydrogenated TiO_{2-x} catalyst and pristine TiO_2.

Oxygen vacancies can adsorb O_2 in the gas phase to form superoxide ions, which are good for the formation of nitro and nitrate groups to promote SCR activity. The oxygen vacancies of catalysts can be determined using PL spectra. Many studies have shown that a larger oxygen vacancy content results in a weaker PL signal. Figure S7 show the PL spectra of pristine TiO_2 and hydrogenated TiO_{2-x}. The oxygen vacancy content of hydrogenated TiO_{2-x} was higher than that of pristine TiO_2. Oxygen vacancies benefit the recombination of photogenerated electron–hole pairs, suggesting a higher separation efficiency of charge carriers and, accordingly, superior catalytic activity for hydrogenated TiO_{2-x}.

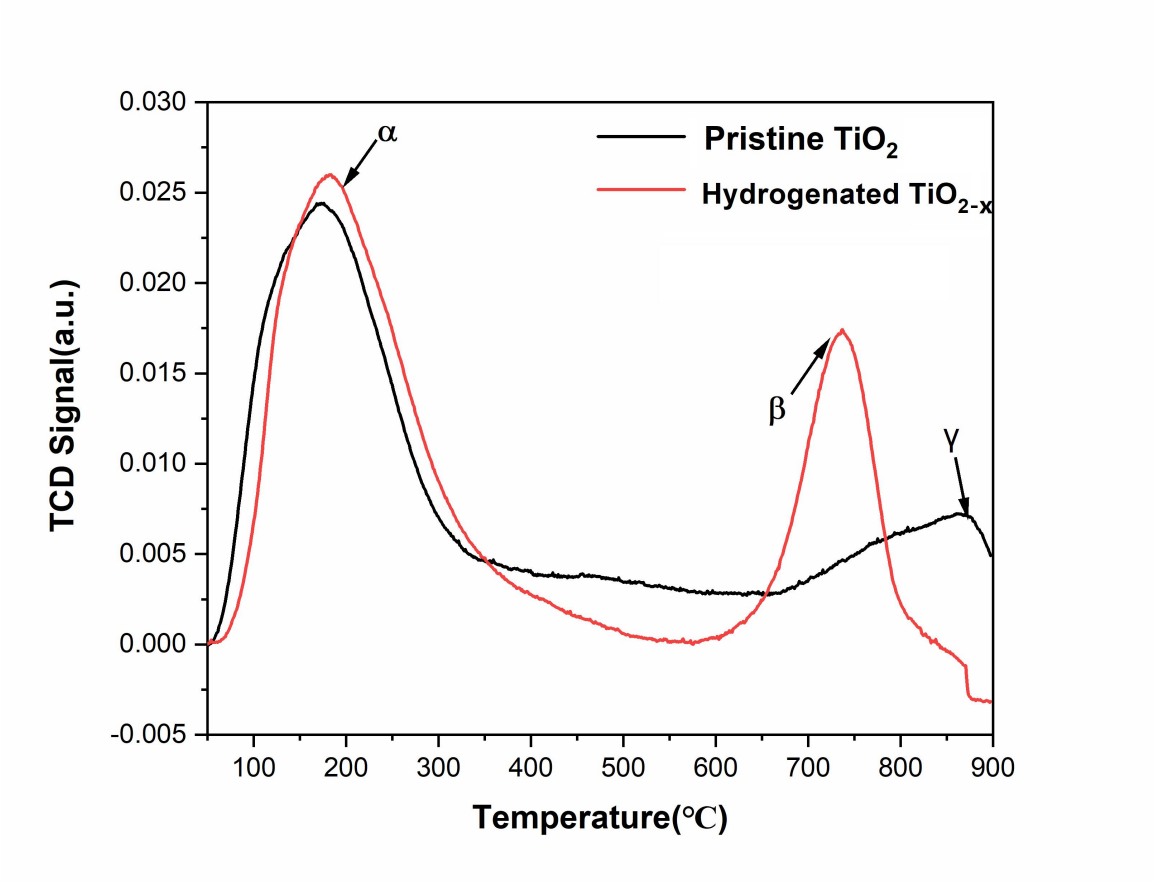

Fig. S8. O_2-TPD profiles of hydrogenated TiO_{2-x} catalyst and pristine TiO_2.

Figure S8 shows O_2-TPD spectra for the pristine TiO_2 and hydrogenated TiO_{2-x} materials. Pristine TiO_2 and hydrogenated TiO_{2-x} featured a strong oxygen adsorption capacity, with a clear oxygen desorption peak (α peak) below 200 ℃. As the temperature was increased, oxygen desorbed from the materials, but the peak shape was unclear. At approximately 600 ℃, a second desorption peak (β peak) appeared for hydrogenated TiO_{2-x}, while a third desorption peak (γ peak) appeared for pristine TiO_2 at temperatures above 800 °C. The first desorption peak temperature of pristine TiO_2 was lower than that of hydrogenated TiO_{2-x}, as shown in Fig. S8, which might correspond to physically adsorbed oxygen or weakly chemisorbed O_2 species. As the temperature increased, the slow desorption process of weakly chemisorbed oxygen occurred. The O_α desorption amount of hydrogenated TiO_{2-x} was greater than that of pristine TiO_2. The second desorption peak occurred at a higher temperature, corresponding to strongly chemisorbed O^- and O_2^{2-}, while the third desorption peak corresponded to chemically stable lattice oxygen. Considering the desorption temperatures, strongly chemisorbed O^{2-}, namely, oxygen species from the second desorption peak, was likely to play a major role in the catalytic process. During the

reaction, the improved desorption properties of chemisorbed O^{2-} on the catalyst contributed to more favorable catalytic reactivity. Catalysts with strong oxygen storage capacity and good oxygen desorption performance might be expected to show high catalytic activity. The chemically stable lattice oxygen sites are mainly derived from TiO_2 and O_2. Chemisorbed O^{2-} arises from interactions between O_2 and TiO_2, with more oxygen defects resulting in more chemically adsorbed oxygen. Therefore, the oxygen deficiency can induce the catalyst surface to more easily desorb chemisorption O^{2-}, which enhances the catalytic reaction efficiency. Therefore, regarding O_β, the hydrogenated TiO_{2-x} catalyst had more chemically adsorbed oxygen compared with pristine TiO_2.

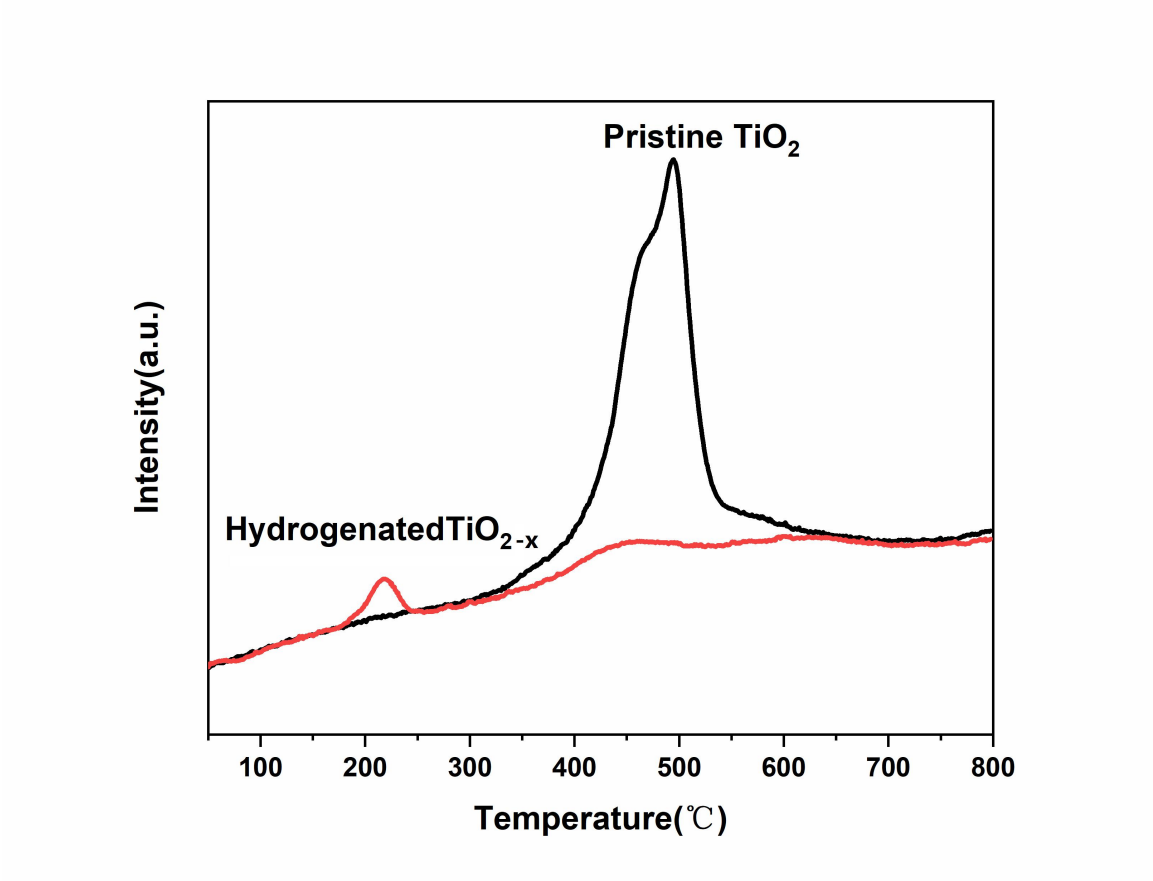

Fig. S9. H_2-TPR profiles of hydrogenated TiO_{2-x} catalyst and pristine TiO_2.

Figure S9 shows the H_2-TPR profiles of pristine TiO_2 and hydrogenated TiO_{2-x}. Pristine TiO_2 exhibited a large H_2 reduction peak at 450–500 °C, which corresponded to the H_2 reduction temperature. This was consistent with our experimental TiO_2 hydrogenation temperature. As shown in Fig. S9, the redox performance of the catalyst increased significantly in the low-temperature zone after hydrogenation. The reduction peaks at 200–300 °C were attributed to the reduction of surface Ti^{4+} ions. Mutual conversion between Ti^{3+} and Ti^{4+} endowed TiO_2 with redox performance, which was another reason for the denitrification performance of hydrogenated TiO_2 being significantly improved.

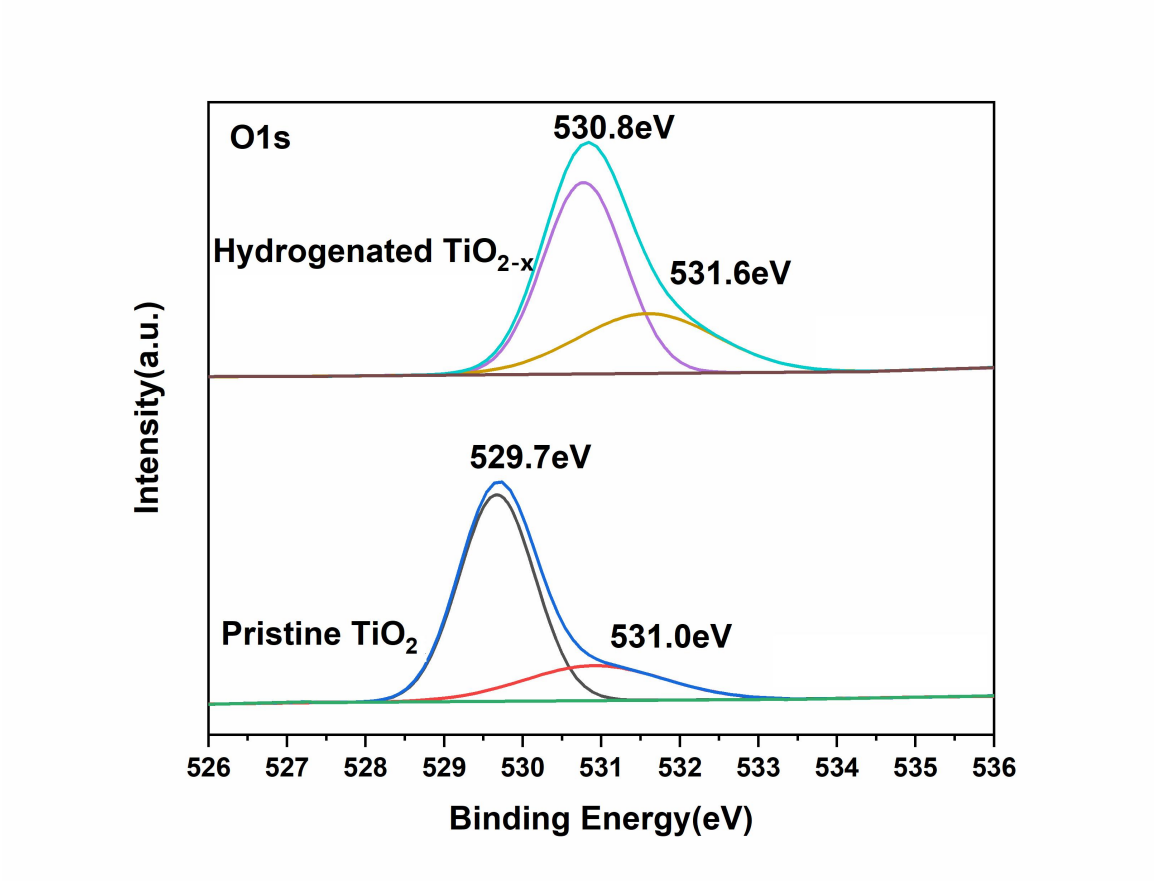

Fig. S10. In-situ XPS spectra of hydrogenated TiO_{2-x} catalyst and pristine TiO_2: O 1s

For better quantitative analysis, changes in the surface chemical bonding of TiO_2 nanocrystals induced by hydrogenation were investigated using in-situ XPS. Figure S10-S12 show the O 1s, Ti 2p, and valence band spectra of pristine TiO_2 and hydrogenated TiO_{2-x}. The O 1s XPS spectra of pristine and hydrogenated TiO_{2-x} showed large differences. The O 1s peaks were resolved into two peaks at about 529.7-530.8 eV and 531.0-531.6 eV for pristine TiO_2 and hydrogenated TiO_{2-x}, respectively. The broader peak at 531.0-531.6 eV was attributed to oxygen adsorbed on the TiO_2 surface. The narrow peak at 529.7-530.8 eV was attributed to Ti–O bonds in the TiO_2 lattice. According to the peak fitting results, the ratio of adsorbed oxygen to lattice oxygen increased from 31.14% in the pristine TiO_2 to 53.46% in the hydrogenated TiO_{2-x}. This variation was primarily the result of the loss of lattice oxygen during the hydrogenation process to

form oxygen vacancies, which subsequently adsorbed ambient water vapor to generate surface hydroxyl groups. This process increased the percentage of adsorbed oxygen in the material.

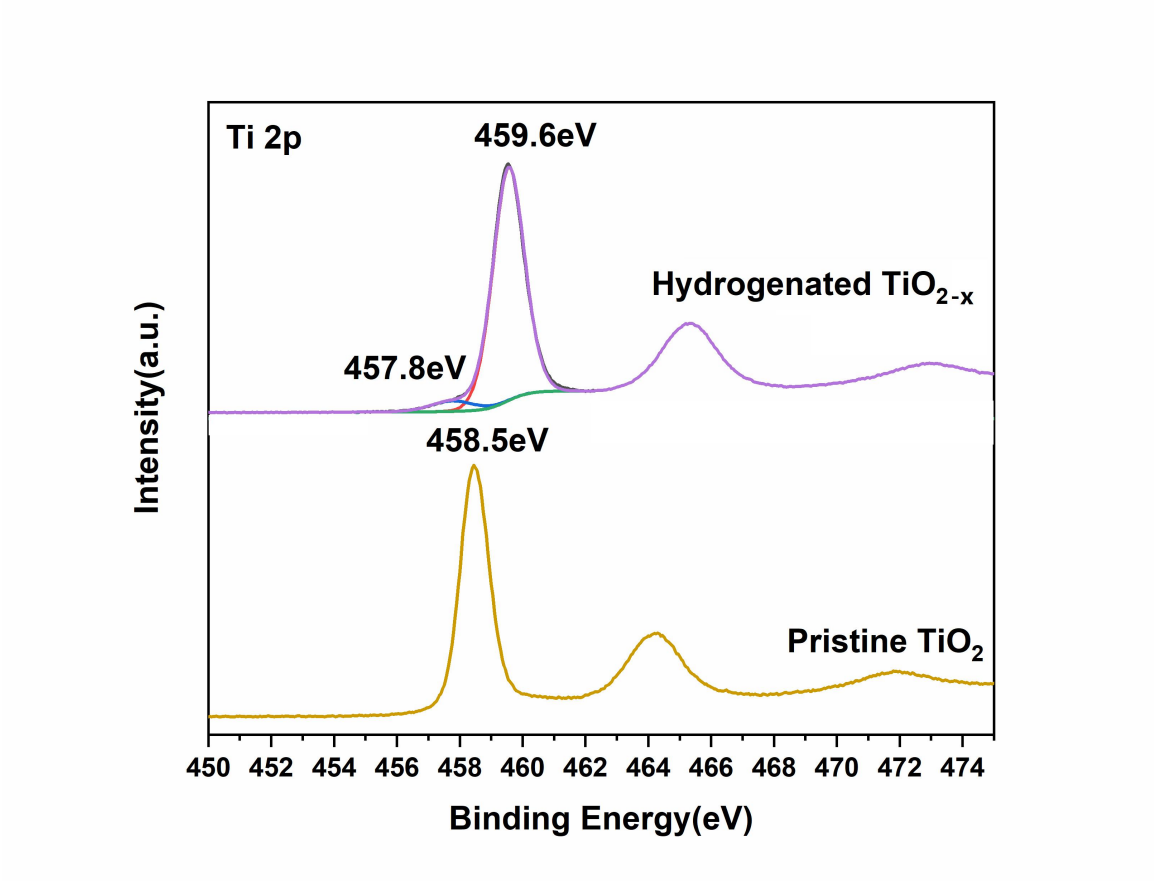

Fig. S11. In-situ XPS spectra of hydrogenated TiO_{2-x} catalyst and pristine TiO_2: Ti 2p

The Ti 2p spectrum of the H-TiO_{2-x} shows a shift in the Ti^{4+} 2p3/2 peak by 1.1 eV toward a higher binding energy, indicating that the Ti in this material gained electrons. This could have been a consequence of electron transfer to surrounding Ti^{4+} during the oxygen vacancy generation process, with the simultaneous formation of Ti^{3+}. After peak fitting, the Ti^{3+}/Ti^{4+} ratio was determined to be 6.15%.

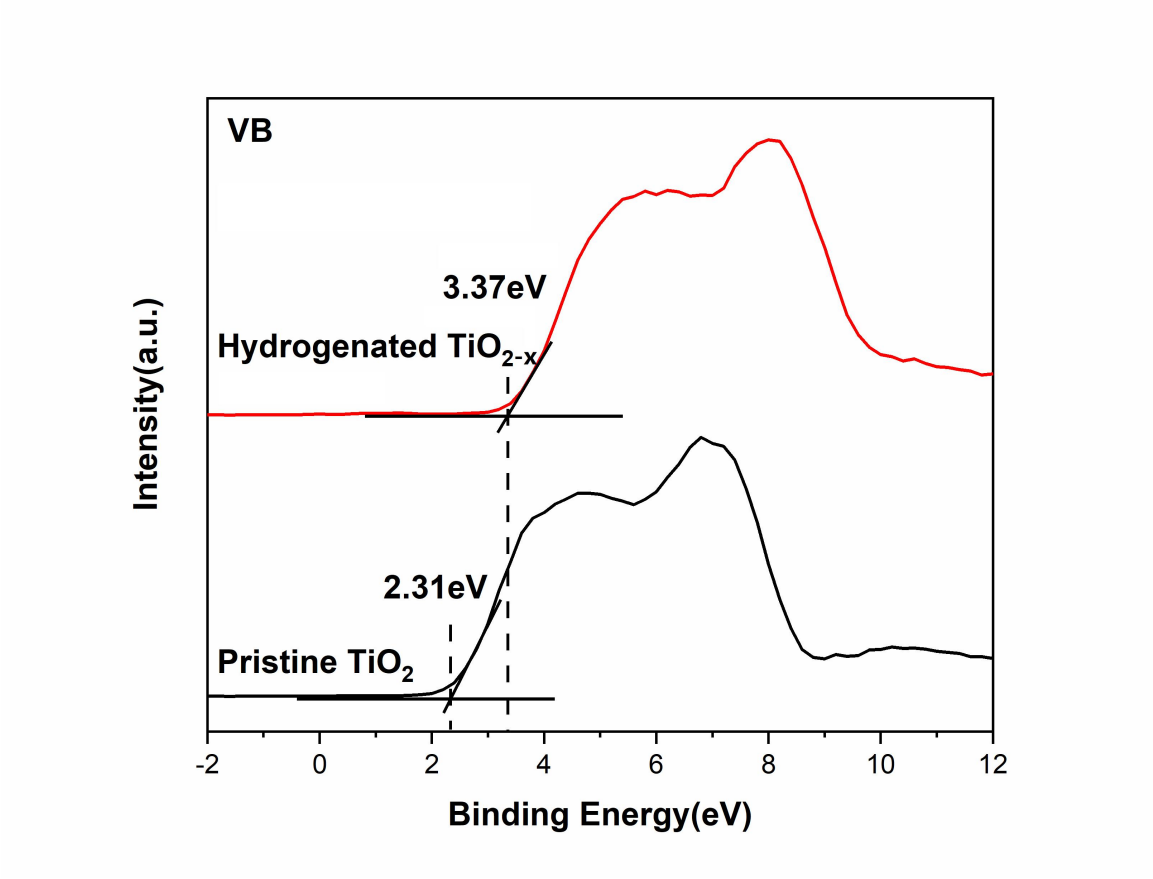

Fig. S12. In-situ XPS spectra of hydrogenated TiO_{2-x} catalyst and pristine TiO_2: valence bands

As shown in Fig. S12, the bottom of the valence band in pristine TiO_2 was positioned at 2.31 eV, and oxidation was weak. After hydrogenation, the bottom of the valence band of hydrogenated TiO_{2-x} was shifted to a higher binding energy of 3.37 eV, indicating that more defects were generated and that oxidation was significantly stronger.

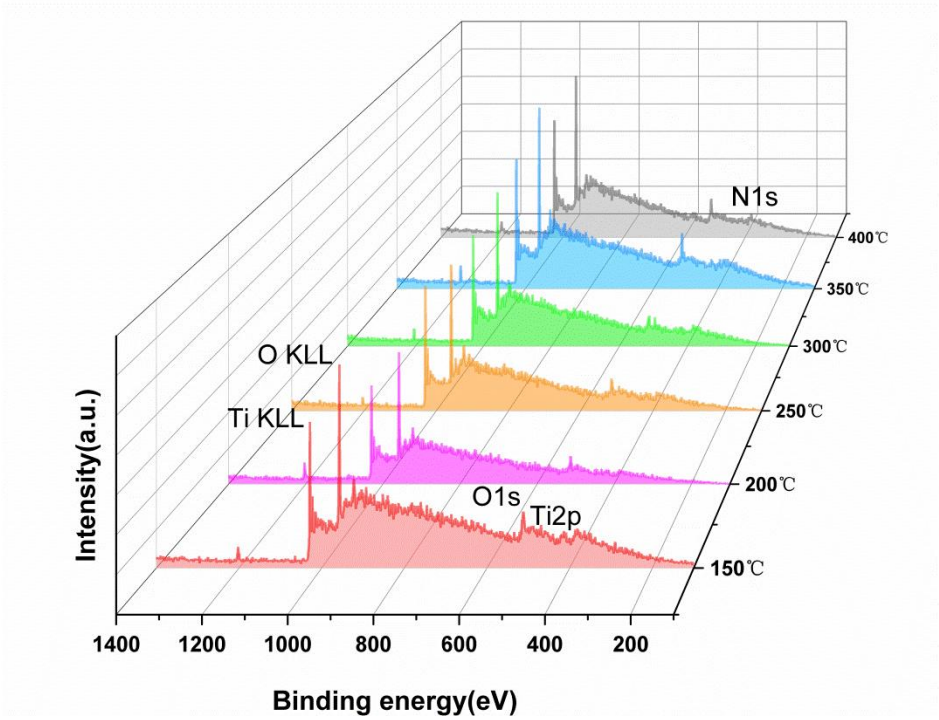

Fig. S13 In-situ XPS spectra of hydrogenated TiO_{2-x} in the NH_3-SCR process at 150–400 ℃: survey spectra.

As shown in Fig. S13, the XPS survey spectra acquired from the H-TiO_{2-x} catalyst during the denitrification process at 150-400 ℃ all contained a N 1s peak near 400 eV. This peak indicates that either nitrogen doping, or the adsorption of N-containing compounds occurred during the denitrification process.

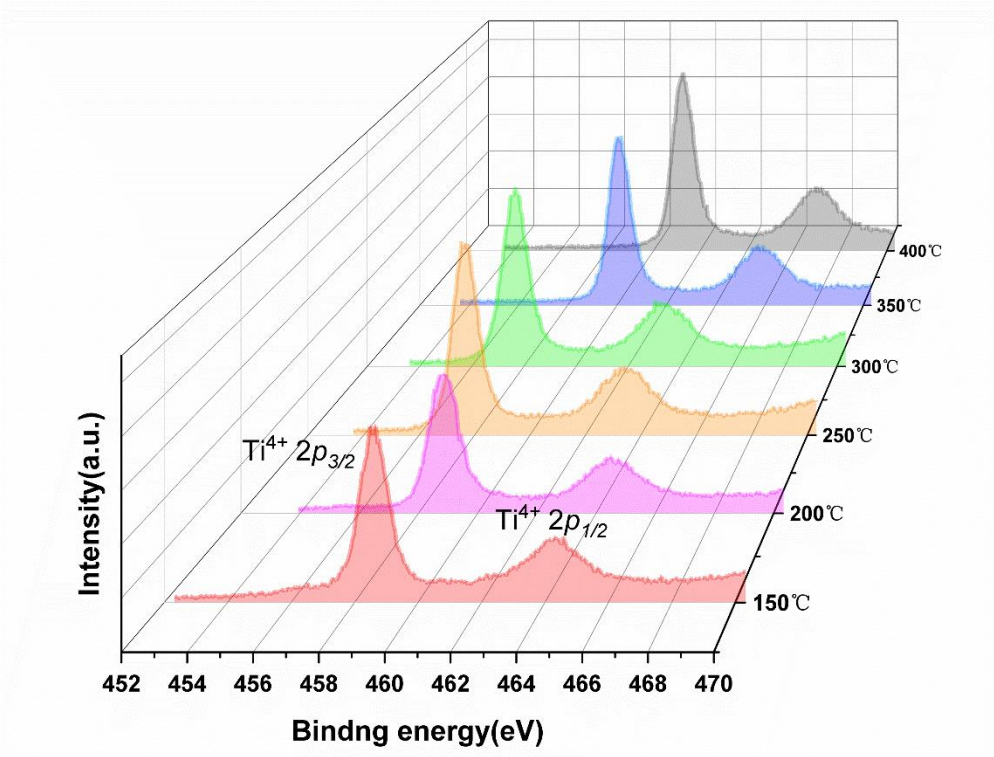

Fig. S14. In-situ XPS spectra of hydrogenated TiO_{2-x} in the NH_3-SCR process at 150–400 ℃: Ti 2p.

Fig. S14 presents the Ti 2p spectrum of the H-TiO_{2-x} in the NH_3-SCR process. During the deNOx process of hydrogenated TiO_{2-x} at 150–400 ° C, the Ti valence state did not change. The Ti spectrum of hydrogenated TiO_{2-x} mainly showed that Ti in hydrogenated TiO_{2-x} mainly existed in the form of Ti^{4+} during the NH_3-SCR process. Compared with freshly hydrogenated TiO_{2-x} catalyst, Ti^{3+} was observed to disappear during the reaction, which might be due to nitrogen doping.

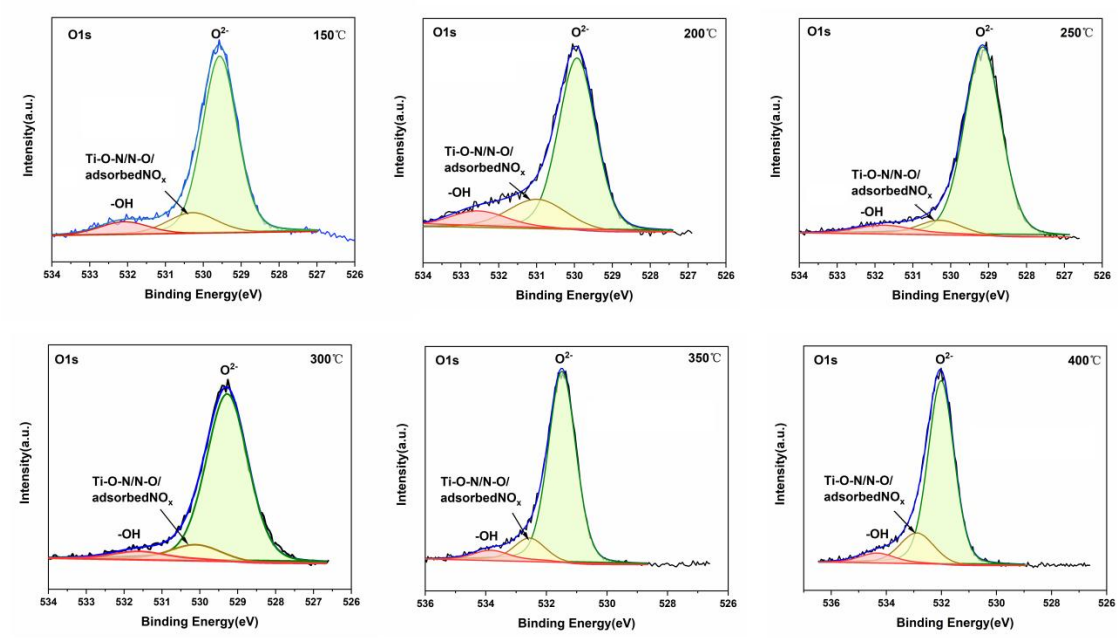

Fig. S15. In-situ XPS spectra of hydrogenated TiO_{2-x} in the NH_3-SCR process at 150–400 ℃: O 1s.

Fig. S15 provides the O 1s spectrum. The O_α peak of O^{2-} in the TiO_2 lattice appeared around 529–530 eV at 150–300 °C, the O_β peak of oxygen adsorbed on TiO_2 appeared around 530–532 eV, and the O_γ peak of surface hydroxyl groups (–OH) on TiO_2 appeared around 532–533 eV. As shown in Table S2, with increasing temperature, the O_β+ O_γ/total O ratio continuously increased from 250 to 400 °C, indicating continuous adsorption of oxygen to supplement the continuous consumption of lattice oxygen by the hydrogenated TiO_{2-x} catalyst. In the NH_3-SCR process, not only adsorbed oxygen on the catalyst surface, but also oxygen in the catalyst body phase, participated in the catalytic reaction. The presence of oxygen defects accelerated the circulation of gaseous oxygen and lattice oxygen on the surface and in the bulk of the catalyst. Oxygen on the catalyst surface was oxidized to active oxygen, which can effectively promote the SCR reaction. Owing to the consumption of surface oxygen, many oxygen vacancies were left on the catalyst surface, which were conducive to oxygen adsorption from the gas phase. Electrons were continuously exchanged through interactions between adsorbed oxygen and metal ions in the active surface components. This exchange maintained the balance of reactive oxygen species involved in the reaction on the catalyst surface.

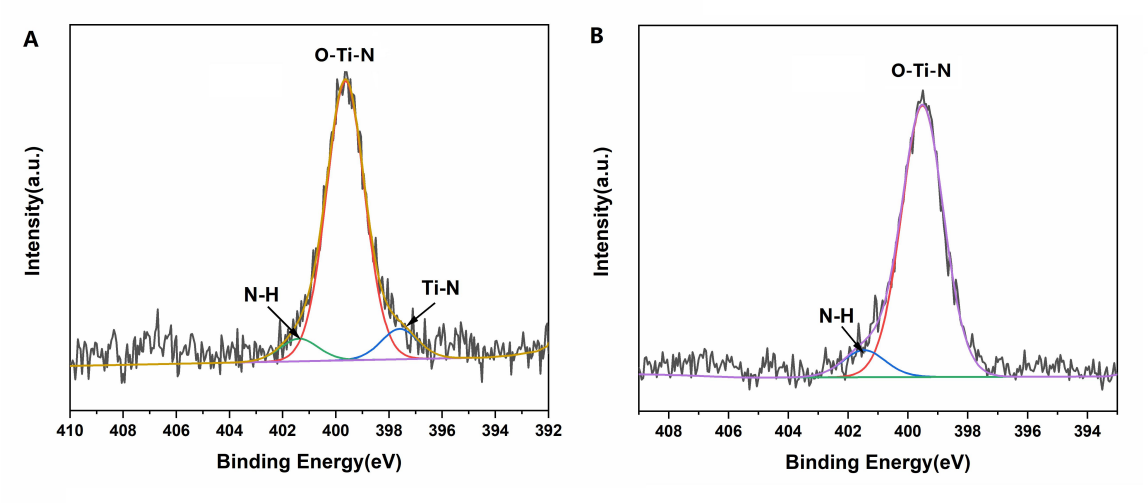

Fig. S16. XPS spectra of the hydrogenated TiO_{2-x} sample. (A) NH_3 atmosphere at 350℃,and (B) $NO+O_2$ atmosphere at 350℃.

Figure S16 demonstrates that nitrogen doping of the H-TiO_{2-x} catalyst surface occurred under both conditions. Previous studies have shown that the nitrogen doping of TiO_2 can proceed under an NH_3 atmosphere at 500 ℃ as N from NH_3 partially replaces lattice oxygen of TiO_2, forming O-Ti-N and oxygen vacancies[1, 2].

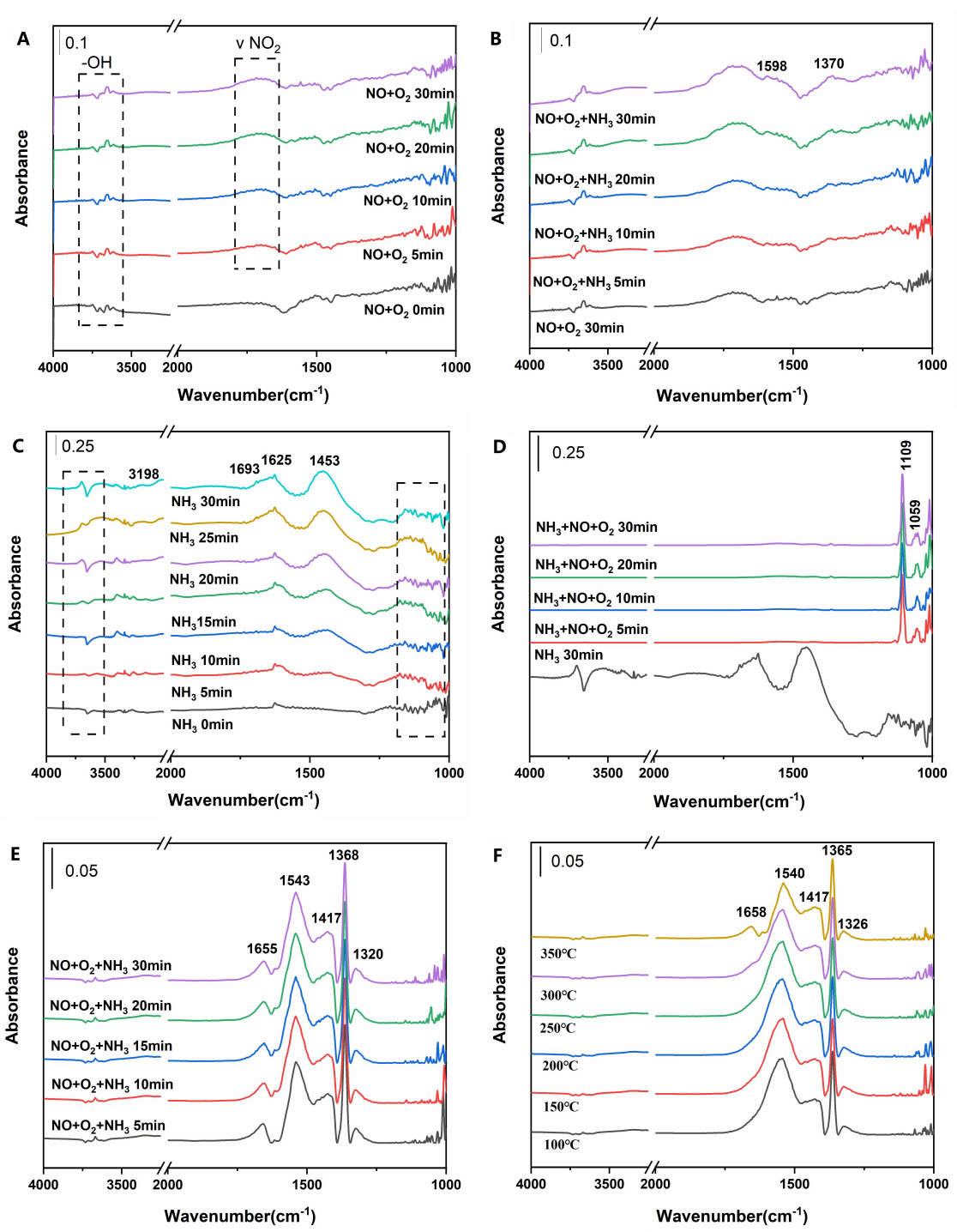

Fig. S17 DRIFT spectra of hydrogenated TiO_{2-x} catalyst. a Exposed to NO and O_2 for various times. b Preabsorbed with NO + O_2 and then treated with NH_3. c Exposed to NH_3 for various times. d Preabsorbed with NH_3 and then treated with NO + O_2. e Exposed to NH_3 + NO + O_2 for 30 min. f With a temperature gradient in NH_3 + NO + O_2 atmosphere

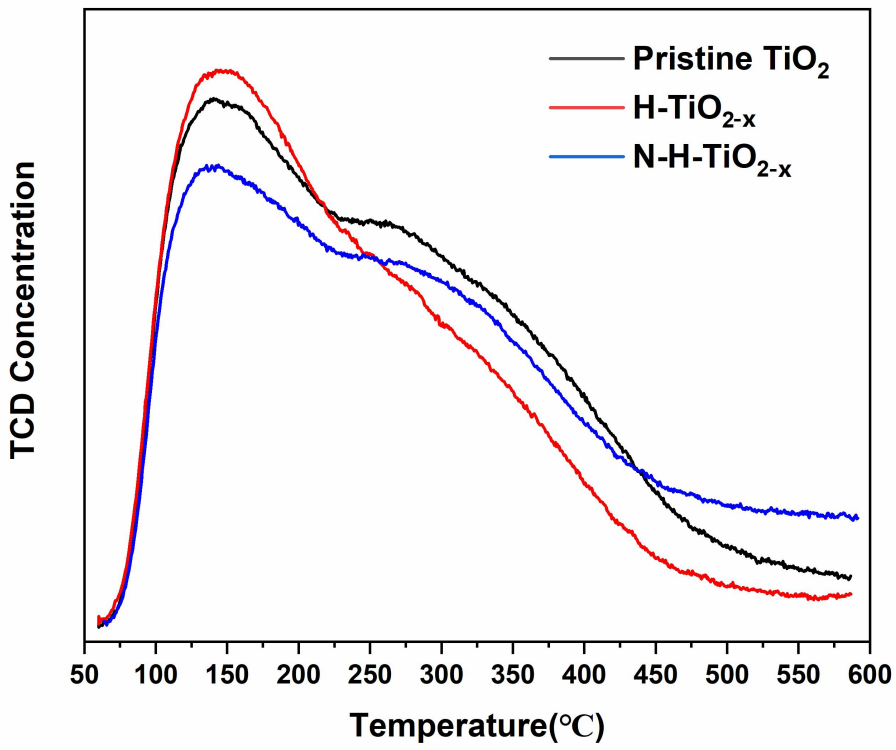

Fig. S18 NH_3-TPD profiles of pristine TiO_2, hydrogenated TiO_{2-x} catalyst and N doped hydrogenated TiO_{2-x}

The results obtained from NH_3-temperature programmed desorption show that the pristine TiO_2 was somewhat acidic and was also able to adsorb NH_3.We used the NH_3-TPD curve peak fitting process to calculate the amount of NH_3 desorbed for each catalyst, and the results are listed in Table S4. It can be seen from Table S4 that according to the integrated area of the NH_3-TPD spectrum, the total acid content is reduced after nitrogen doping, indicating that nitrogen doping reduces the acidity of the hydrogenated TiO_{2-x} catalyst. This may be related to the N doping filling up part of the oxygen vacancies, resulting in a decrease in oxygen vacancies and a decrease in acidity.

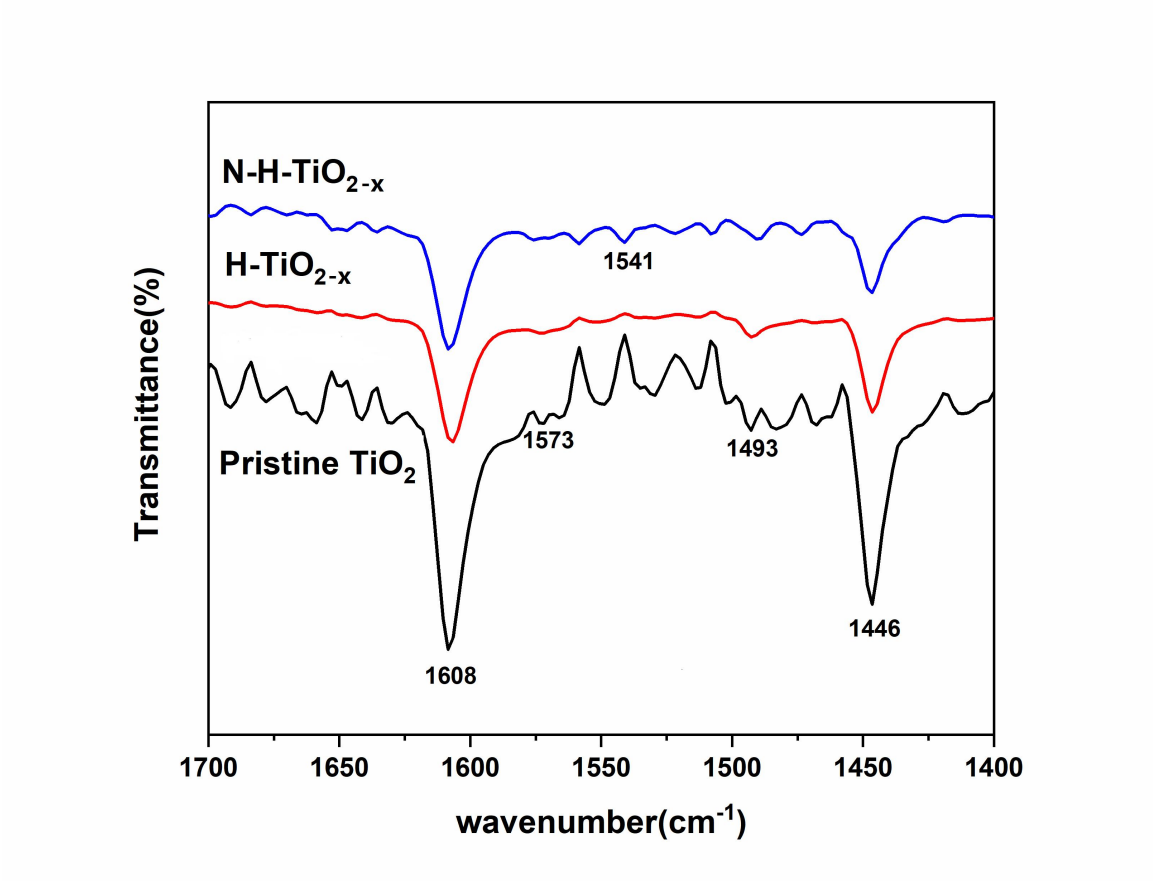

Fig. S19 Py-IR spectra of pristine TiO_2, hydrogenated TiO_{2-x} catalyst and N doped hydrogenated TiO_{2-x}

The results obtained from pyridine adsorption infrared spectroscopy show that the pristine TiO_2 was somewhat acidic and was also able to adsorb NH_3.The peaks at wave numbers of 1608 cm^{-1}, 1573 cm^{-1}, 1493 cm^{-1}, and 1446 cm^{-1} are the peaks of L acid sites, and the peaks at 1541 cm^{-1} maybe the peaks of B acid sites or the noise peak. Table S5 shows the pyridine infrared curve fitting results of pristine TiO_2, hydrogenated TiO_{2-x} and N-TiO_{2-x} catalysts. It can be seen from Figure S19 and TableS5 that the acidic and the acid strength is obviously weakened after hydrogenation and nitrogen doping. The acidity of pristine TiO_2 may be caused by the small amount of impurities such as S and P (Table S1). The content of S and P in hydrogenated TiO_{2-x} is greatly reduced (Table S1). The L acid is mainly caused by oxygen vacancies caused by surface defects of the sample. After the hydrogenated TiO_{2-x} is doped with nitrogen, the L acid is reduced, indicating that the nitrogen doping has filled part of the oxygen vacancies, which is consistent with the results of NH_3-TPD. It can be seen that the total acidity of hydrogenated TiO_2 is reduced after nitrogen doping. It shows that N doping reduces the acidity of the catalyst.

Table S1 Chemical composition analysis results of pristine titanium dioxide and hydrogenated TiO_{2-x}.

wt %	SiO_2	P_2O_5	SO_3	Cl	CaO	TiO_2	ZrO_2	Nb_2O_5
Pristine TiO_2	0.022	0.181	1.775	0.016	0.031	97.921	0.017	0.037
Hydrogenated TiO_{2-x}	0.939	0.187	0.288	0.027	0.159	98.019	0.018	0.040

The pristine TiO_2 powder is primarily composed of TiO_2 with traces of SO_3, P_2O_5 and Cl. Hydrogenation drastically reduces SO_3 but does not affect the other impurities.

Table S2 Binding energies and surface atomic concentrations of N and O in hydrogenated TiO_{2-x} catalysts at 150–400 °C.

samples	Bing Energy (eV) and surface atomic concentrations (%)									
	O 1s					N 1s				
	Oα/eV	Oβ/eV	Oγ/eV	(Oβ+ Oγ)/O	Surface concentration (%)	Ti-O-N/eV	N-H/eV	N-O/eV	Ti-O-N / N	Surface concentration (%)
150℃	529.7	530.42	532.22	21.36%	63.72	399.40	400.90	406.76	45.11%	0.23
200℃	529.93	530.99	532.55	28.77%	63.89	399.67	401.36	406.89	53.67%	0.28
250℃	529.98	531.12	532.61	12.33%	64.01	398.92	400.50	406.06	58.24%	0.31
300℃	530.09	531.1	532.42	13.40%	63.55	398.95	——	406.09	75.75%	0.38
350℃	529.99	531.07	532.25	15.35%	64.67	401.35	——	408.38	78.54%	0.45
400℃	532.01	532.89	534.34	21.60%	64.49	402.61	——	——	100%	0.44

Table S3 EXAFS fitting parameters at the Ti K-edge for various samples (S02 = 0.73).

Sample	Shell	N^a	R(Å)^b	$\sigma^2\times10^3$(Å^2)^c	ΔE_0 (eV)^d	R factor
TiO_2	Ti-O	6*	1.96±0.02	6.3±2.3	-1.8±2.6	0.008
Hydrogenated TiO_{2-x} catalyst	Ti-O	5.9±0.8	1.92±0.01	3.4±2.7	-2.5±0.7	0.002
	Ti-Ti	5.5±1.5	3.23±0.02	44.2±6.2		
N-Hydrogenated TiO_{2-x} catalyst	Ti-O	6.1±1.2	1.91±0.01	6.5±3.5	-3.7±1.0	0.004
	Ti-Ti	7.7±3.6	3.23±0.03	72.3±12.8		

[a]N, coordination number; [b]R, bond distance; [c]σ^2, Debye-Waller factor; [d] ΔE_0, inner potential correction; R factor, goodness of fit.

Table S4 NH_3 desorption amount of pristine TiO_2, H-TiO_{2-x} and N-H-TiO_{2-x}

Samples	Weak adsorption NH_3		Strong adsorption NH_3		Total NH_3 desorption amount(mmol/g)
	Temperature peak (℃)	NH_3 desorption amount(mmol/g)	Temperature peak (℃)	NH_3 desorption amount(mmol/g)	
Pristine TiO_2	135.4	0.37231	311.2	0.25778	0.63009
H-TiO_{2-x}	138.9	0.38470	295.9	0.18007	0.56477
N-H-TiO_{2-x}	132.3	0.31102	295.0	0.20632	0.51734

Table S5 Pyridine infrared adsorption amount of pristine TiO_2,H-TiO_{2-x} and N-H-TiO_{2-x}

Samples	Lewis acid	Bronsted acid	Total acid amount（mmol/g）
	Acidity amount(mmol/g)	Acidity amount(mmol/g)	
Pristine TiO_2	5.163	——	5.163
H-TiO_{2-x}	2.527	——	2.527
N-H-TiO_{2-x}	2.183	0.249/——	2.432

References

1. Asahi, R., Morikawa, T., Ohwaki, T., Aoki, K., Taga, Y. Visible-light photocatalysis in nitrogen doped titanium oxides, *Science*, **293**,269-271(2001).
2. Foo, C. et al., Characterisation of oxygen defects and nitrogen impurities in TiO_2 photocatalysts using variable-temperature X-ray powder diffraction. *Nat. Commun.* **12**,661(2021).
3. Leedahl, B., de Boer, T., Yuan, X., Moewes, A. Oxygen vacancy induced structural distortions in black titania: a unique approach using soft X-ray EXAFS at the O-K edge, *Chem.–A Eur. J.* **25**, 3272-3278 (2019).
4. Yoshida, T., et al., Quantitative XAFS/EELS analyses of nitrogen species in titanium oxide photocatalysts. *Surf Interface Anal.* **1-5**(2018).